ARMY RESEARCH LABORATORY

A 37-mm Ceramic Gun Nozzle Stress Analysis

by Xiaogang Huang, James Garner, and Paul Conroy

ARL-TR-3804 **May 2006**

NOTICES

Disclaimers

The findings in this report are not to be construed as an official Department of the Army position unless so designated by other authorized documents.

Citation of manufacturer's or trade names does not constitute an official endorsement or approval of the use thereof.

Destroy this report when it is no longer needed. Do not return it to the originator.

Army Research Laboratory
Aberdeen Proving Ground, MD 21005-5066

ARL-TR-3804 **May 2006**

A 37-mm Ceramic Gun Nozzle Stress Analysis

Xiaogang Huang, James Garner, and Paul Conroy
Weapons and Materials Research Directorate, ARL

REPORT DOCUMENTATION PAGE

Form Approved
OMB No. 0704-0188

1. REPORT DATE *(DD-MM-YYYY)*	2. REPORT TYPE	3. DATES COVERED (From - To)
May 2006	Final	October 2005–September 2006

4. TITLE AND SUBTITLE
A 37-mm Ceramic Gun Nozzle Stress Analysis

5a. CONTRACT NUMBER

5b. GRANT NUMBER

5c. PROGRAM ELEMENT NUMBER

6. AUTHOR(S)
Xiaogang Huang, James Garner, and Paul Conroy

5d. PROJECT NUMBER
622618.H8011

5e. TASK NUMBER

5f. WORK UNIT NUMBER

7. PERFORMING ORGANIZATION NAME(S) AND ADDRESS(ES)
U.S. Army Research Laboratory
ATTN: AMSRD-ARL-WM-BC
Aberdeen Proving Ground, MD 21005-5066

8. PERFORMING ORGANIZATION REPORT NUMBER
ARL-TR-3804

9. SPONSORING/MONITORING AGENCY NAME(S) AND ADDRESS(ES)

10. SPONSOR/MONITOR'S ACRONYM(S)

11. SPONSOR/MONITOR'S REPORT NUMBER(S)

12. DISTRIBUTION/AVAILABILITY STATEMENT
Approved for public release; distribution is unlimited.

13. SUPPLEMENTARY NOTES

14. ABSTRACT
A series of shooting tests was conducted on a 37-mm gun fixture with ceramic nozzles. The primary concern for the design and test of the ceramic nozzle is the combination of the thermal stress and dynamic ballistic stress during the launch. On the basis of previous thermal analysis, a transient sequentially coupled finite-element model is performed to investigate the thermal stresses due to the large temperature gradient and coefficient mismatch of thermal expansion between the ceramic nozzle and the steel holder. The fully-coupled thermal stress analysis is conducted for verification. A DYNA3D model is used to perform the dynamic stress analysis due to the interior ballistic load on the ceramic nozzle. Three candidate ceramic materials, SN47, STK4, and ZRO2, are investigated and compared with the conventional steel nozzle. All the stress components from both thermal and dynamic loads are determined. These predictions are significant to the selected ceramic materials for the nozzle design.

15. SUBJECT TERMS
ceramic nozzle, thermal stress, dynamic stress, thermal erosion

16. SECURITY CLASSIFICATION OF:			17. LIMITATION OF ABSTRACT	18. NUMBER OF PAGES	19a. NAME OF RESPONSIBLE PERSON
a. REPORT	b. ABSTRACT	c. THIS PAGE			Xiaogang Huang
UNCLASSIFIED	UNCLASSIFIED	UNCLASSIFIED	UL	28	19b. TELEPHONE NUMBER (*Include area code*) 410-278-6142

Contents

List of Figures

List of Tables

1. Introduction

Compared with the traditional gun steel nozzle, the ceramic nozzle can sustain higher combustion temperatures and maintain structural integrity. It has great potential to be used in a variety of gun structures (*1*). However, test results showed some surface cracking on the ceramic nozzles. Initial analysis indicated that the excessive thermal stresses during firing lead to compressive strains in the nozzle which can cause cracking when it cools (*2*). In fact, the dynamic, ballistic impact when firing has the same stress level as that produced by the thermal stress. The surface failure should be considered as arising from the combination of both stresses. In order to quantify the failure stresses, it was necessary to conduct a stress analysis. Finite element models (FEMs) are used to simulate the ceramic nozzle thermal and dynamic stress. In the first section, a three-dimensional (3-D) ABAQUS (*3*) model is built to predict the transient thermal stress. The model is sequentially-coupled because the stress deformation is small enough that it does not affect the next heat conduction step. If the thermal deformation is not negligible, a fully-coupled model should be used. For verification purposes, an analysis using a fully-coupled model was also conducted and compared with the sequentially-coupled model results. In the second section, a DYNA3D (*4*) model is also used to determine the nozzle response from the internal ballistic load.

2. Ceramic Nozzle Structure and Materials

In the test, a ceramic nozzle composed of steel and ceramic sections is mounted in the 37-mm gun fixture as shown in figure 1. The steel nozzle section rests on the shoulder of the chamber. A metal rupture disk and spacer are tightened against the nozzle by a threaded retainer. The disk breaks during firing and releases the chamber pressure. The ceramic nozzle inner radius is 6.35 mm and the outer radius is 12.7 mm. The ceramic nozzle thickness is 12.7 mm. Three ceramic materials were selected for study; the steel nozzle was used as a comparison baseline. The detailed mechanical properties and coefficient of thermal expansions (CTE) of these candidate ceramics and the test fixture model components are listed in table 1.

3. Sequentially-Coupled and Fully-Coupled Thermal Stress FEM Analysis

The commercially available finite-element code ABAQUS (*3*) was used to model the full-scale test fixture. The transient thermal stress precedes the thermal deformation determination. If such deformations are relatively small such that they do not change the following heat transfer

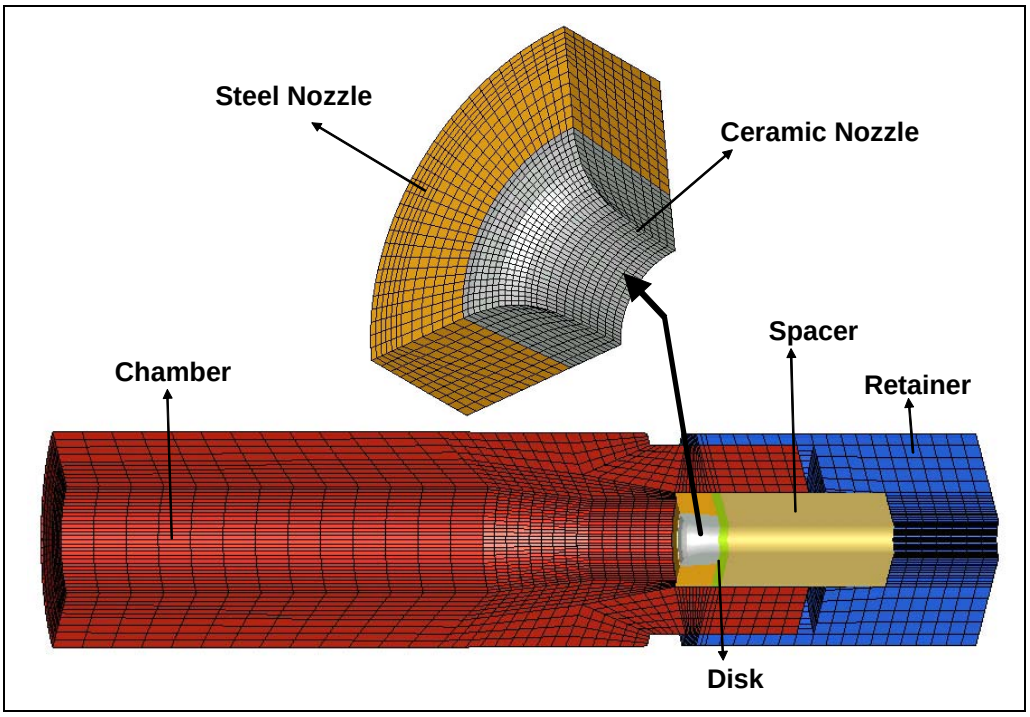

Figure 1. Schematic details of the ceramic nozzle.

Table 1. The material and mechanical properties of the model components.

Part Name	Material	Modulus (GPa)	Poisson's Ratio	Density (kg/m^3)k	CTE ($1/C^o$)
Chamber	Steel	207	0.3	0.039	8.4
Disk	Steel	207	0.3	0.101	8.4
Spacer	Steel	207	0.3	0.697	8.4
Retainer	Steel	207	0.3	0.283	8.4
Ceramic nozzles	SN47	310	0.27	0.283	3.2
	STK	300	0.25	0.043	3.3
	ZRO2	210	0.23	0.039	11.8

analysis iteration, the heat conduction can be calculated independently for the firing cycle. Based on this temperature history, the thermal stress simulation can then be conducted for the same time period. This simulation procedure is called sequentially-coupled thermal stress analysis. If the thermal stress deformation is large enough, the fully-coupled thermal stress analysis must be applied for subsequent heat transfer as a function of the stress deformation. Since the fully coupled simulation requires approximately 10× more computing time than that of sequentially-coupled simulation, it is recommended to adopt sequentially coupled analysis whenever possible (*3*).

The main FEM work for the modeling is inputting the mechanical and geometric data, i.e., constructing nodes and elements, and applying interface and boundary conditions.

The model input includes geometric data, mechanical properties, and temperature histories. The space and time dependent temperature resultant profiles for steel, silicon nitride (SN47), sialon (STK4), and zirconia (ZRO2) ceramic nozzles from Huang et al. (*5*) are used as input histories here. The thermal stress simulations follow these temperature profiles. The mechanical properties of each ceramic nozzle are provided in Swab and Wereszczak (*1*) and steel-parts properties are available from the engineering handbook (*6*) and shown in table 1.

ABAQUS (*3*) keywords were used to generate the nodes and elements. The keyword input is more effective to conduct parametric studies. Four node axisymmetric elements were chosen for the analysis. Extra care was taken in meshing each part of the model, with regard to their common edges. Dense meshes were placed near the nozzle surface area due to the large temperature gradients there. Figure 2 shows the axisymmetric, thermal stress model. There are about 75,000 elements total in the model. The sequentially-coupled thermal stress model requires that the node and element meshing be exactly the same as that in the heat conduction analysis (*5*).

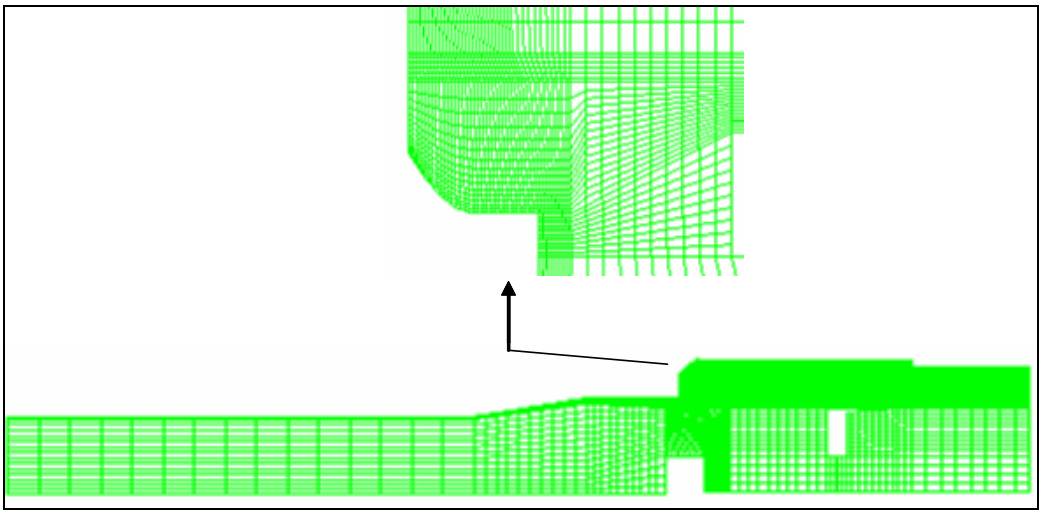

Figure 2. Axisymmetric thermal stress model.

The test chamber end nodes have fixed boundary conditions applied such that they cannot move in any direction. The retainer and spacer are considered perfectly connected to the chamber. This equates to the elimination of thread gaps. The nozzle and steel disk share the common nodes and are in contact and connected to the fixture.

The firing cycle lasts about 30 ms. The maximum centerline gas temperature is 2700 ºC and occurs at 13 ms into the firing sequence. The time increment used in the modeling is 0.2 ms.

4. Ceramic Nozzle Thermal Stress Response

In the thermal stress analysis, the conventional steel nozzle was used as a baseline. The SN47, STK2, and ZRO4 ceramics were selected as candidate materials for the nozzle analysis. For analysis and comparison convenience, the Huang et al. (*5*) temperature gradient under the steel nozzle surface and the surface temperatures for the steel and ceramic nozzles are plotted in figures 3 and 4, respectively. For the all-steel nozzle, the temperature 0.1 mm below the surface is 450 °C cooler. Intuitively, the hot nozzle surface expansion is restrained by the inside cooler materials. The large thermal gradients cause compression stresses near the surface. For the different ceramic materials, the surface temperatures are varied as shown in figure 4. The ZRO2 ceramic nozzle has the highest temperature at 2100 °C, while the baseline material steel nozzle has the lowest temperature at 1750 °C.

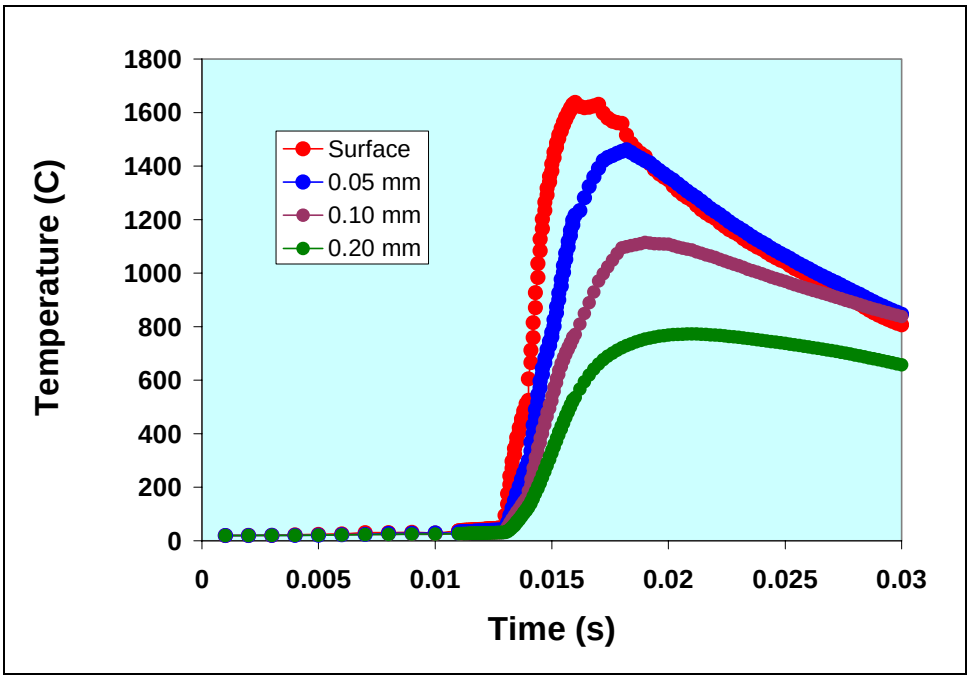

Figure 3. Temperature gradient near the steel nozzle surface.

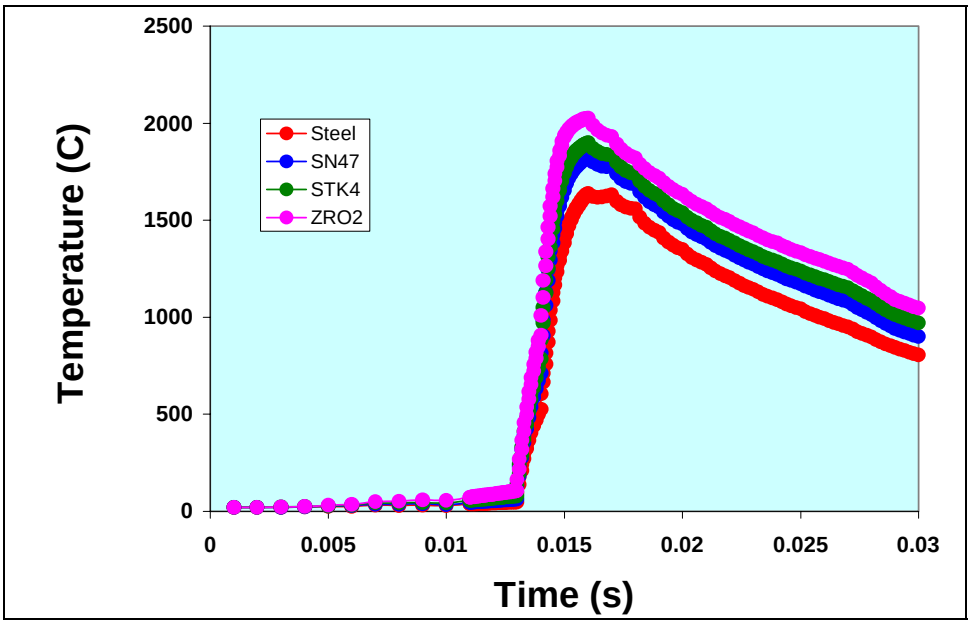

Figure 4. Surface temperatures for the ceramic nozzles.

Figure 5 shows each transient thermal surface stress component response of the steel nozzle. The hoop stress reaches its peak value at 3000 MPa in compression and the axial stress reaches its peak value at 1950 MPa at the in-bore time of 16 ms. The peak in-plane shear stress and radial stress are relatively small at 1000 and 600 MPa, respectively. More details of the hoop stress and in-plane shear stress are discussed for each nozzle material.

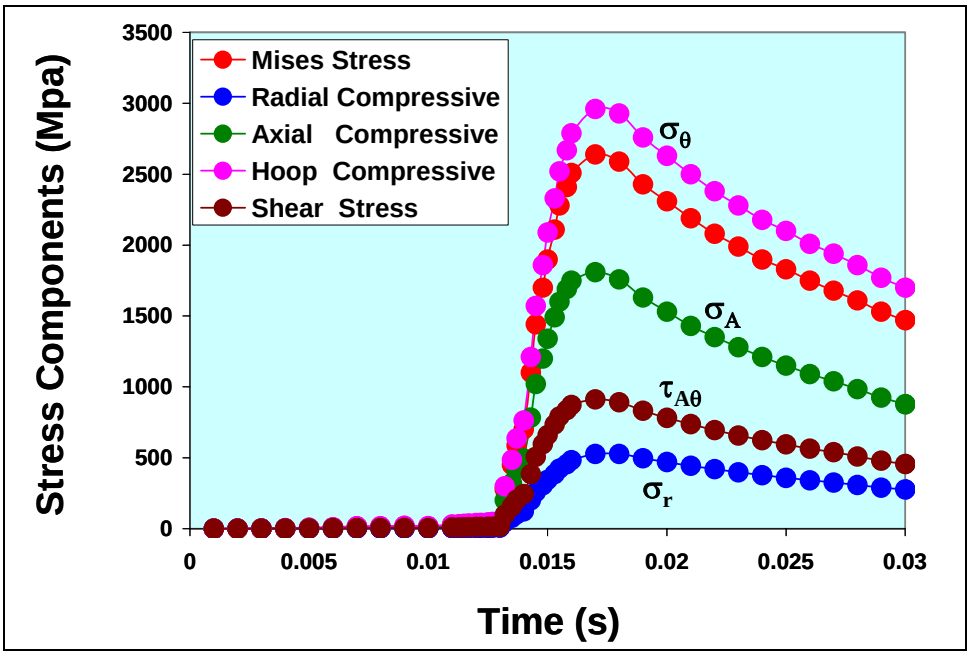

Figure 5. Thermal surface stress components for the steel nozzle.

Figure 6 shows the hoop contours for the steel and ceramic nozzles at their peak values. The thermal compression stress areas are limited to near the surfaces. ZRO2 ceramic shows 4000 MPa hoop stress, which is much higher than those of ceramic nozzles SN47 and STK4, which have stresses of 1850 and 1600 MPa, respectively. The surface hoop stress profiles of these nozzles are plotted in figure 7. The thermal hoop stresses of SN47 and STK4 are less than that of the steel nozzle.

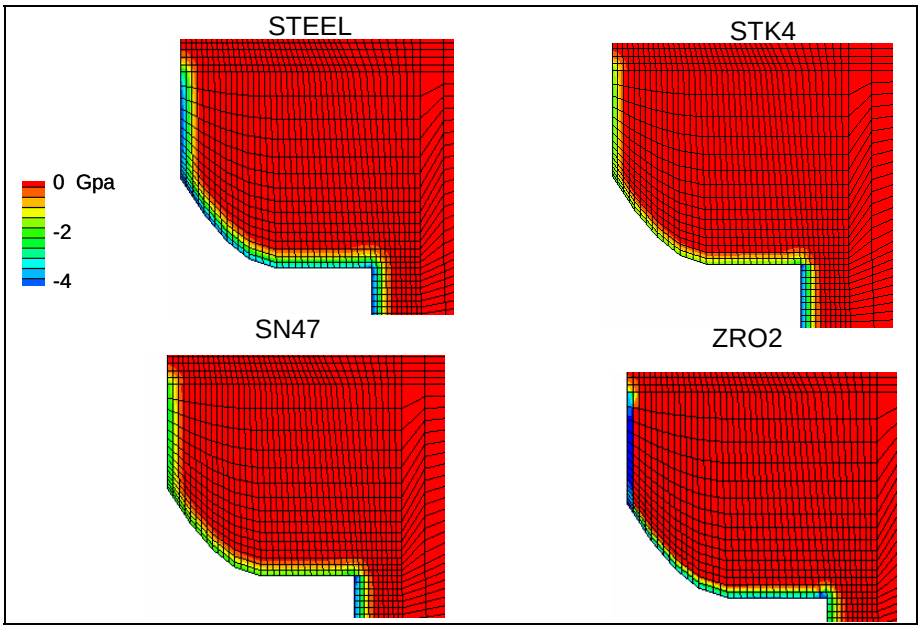

Figure 6. The hoop stress contours for the steel and ceramic nozzles at peak values.

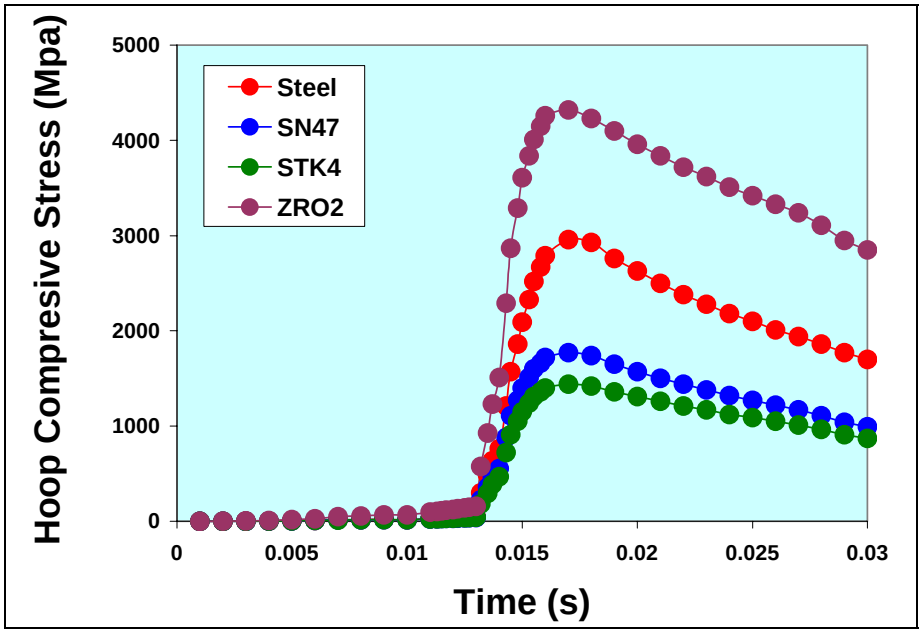

Figure 7. The thermal hoop stress profiles for the steel and ceramic nozzles.

The brittle ceramics have significant compressive material strength but are susceptible to tensile and shear stresses. For design purposes, the shear stress requires investigation. Figure 8 shows the shear stress profiles of the four nozzles. Although the shear stresses are much smaller compared to the hoop stresses, the shear stresses may cause tension failures along the surface 45° directions according to stress status theory (*7*). The ceramic material shear strength must also be examined for the nozzle designs. In the current cases, the 3-D principle stresses of the ceramic nozzles are all in compression; the complicated 3-D thermal stress states are all in compression regardless of shear stress.

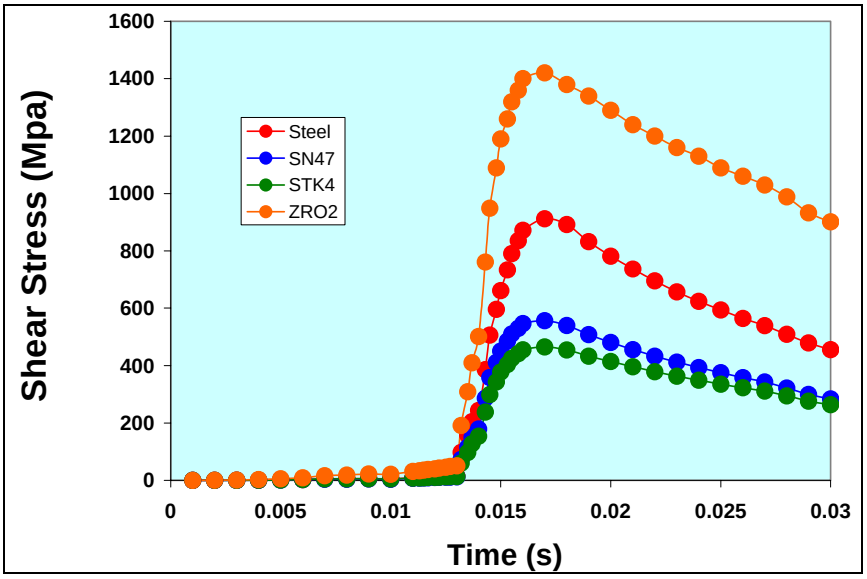

Figure 8. The thermal shear stress profiles for the steel and ceramic nozzles.

5. Ceramic Nozzle Dynamic FEM

In the dynamic FEM analysis, the basic simulation procedure is the same as that in the thermal FEM analysis. DYNA3D, developed by Lawrence Livermore National Laboratory (*4*), was used as the FEM code. In the input data, the internal ballistic pressure is identified (*8*) and used as the DYNA3D loading. The dynamic FEM is shown in figure 1. The corresponding mechanical properties of the model parts and ceramic nozzles are given in table 1. In the model, the interfaces among the chamber, spacer, and retainer are fixed. The nozzle and steel disk are in contact between the chamber shoulder and the spacer. Commercially-available preprocessing software MSC_PATRAN* was used to generate the model. Three-dimensional 8-node Hex8 brick elements were used in the model. Once again, additional care was taken for meshing each part of the model along their common edges. There are approximately 37000 solid elements and

*PATRAN is a registered trademark of MSC Software Corporation, Los Angeles, CA.

45000 nodes total in the DYNA3D model. The model was generated using a PATRAN script file, which lends itself easily to parametric studies. The impact loading time is about 5 ms (see figure 9). The maximum pressure is 350 MPa and occurs at 25 ms into the launch.

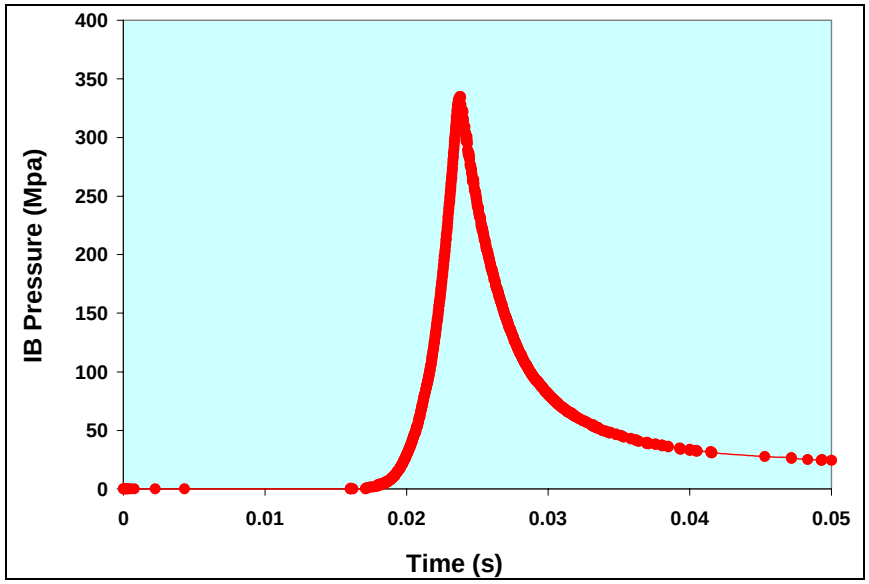

Figure 9. The internal ballistic load on the ceramic nozzles.

In the FEM simulation, data are saved every 0.5 ms for a total of 50 ms. A complete 32-bit simulation requires about 40 hr of CPU time on an SGI Origin 3000 server series or 22 hr on a Linux Powell server. In the analysis of the results, the focus is placed on the ceramic nozzle stress distributions and profiles (peak values). The combinations of both thermal and dynamic loads are considered in the material selection criteria. The post-process software HYPERVIEW* was used to generate the stress contours of the ceramic nozzles and stress wave animations during the firing cycle.

6. Ceramic Nozzle Dynamic Responses and Discussions

In the stress analysis, the peak stress contours are examined in order to determine the locations of the compressive or tensile stresses. The polar stress components are obtained and plotted in a Cartesian coordinate frame (explained in the appendix). As shown in figure 10, the hoop stress varies from compression in the top entrance area to tension in the bottom area. The tension hoop stress reaches it highest value at 700 MPa, especially in the inner bottom corner. This tensile stress is dominant for the nozzle cracking. The radial, axial, and shear stress are quite small and well below the material strength. In the dynamic analysis, the hoop tensile stress determines the ceramic nozzle failure criteria.

*HYPERVIEW, version 7.0, is a registered trademark of Altair Engineering, Troy, MI.

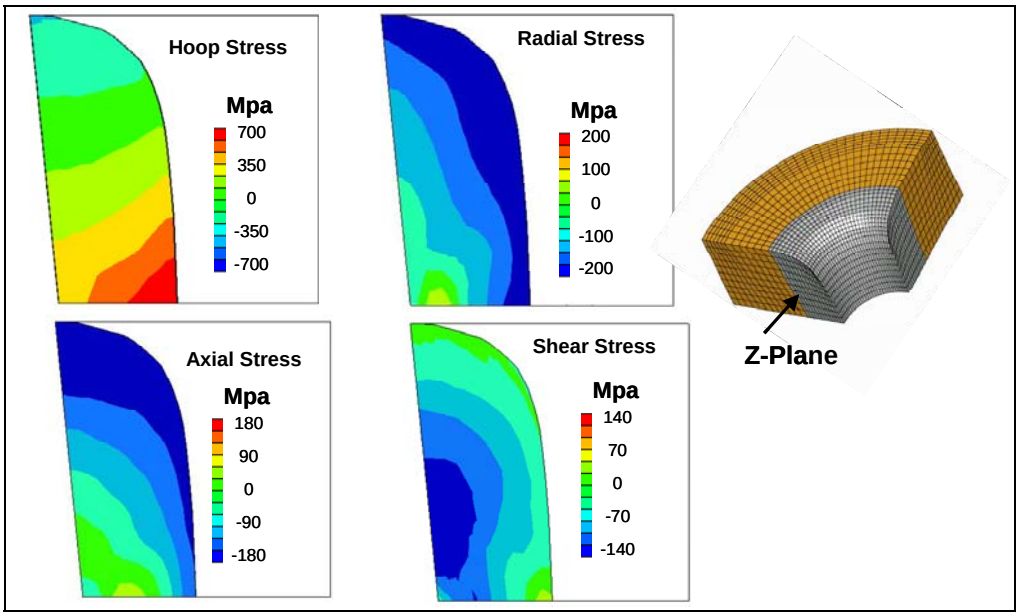

Figure 10. The stress component contours at the peak time for the steel nozzle plotted in the z-plane (see the appendix).

Figure 11 shows the peak hoop stress contours for steel and ceramic nozzles. The hoop stress distributions for the SN47, STK4, and ZRO2 nozzles are basically the same. The nozzle entrance areas are subjected to compression. The nozzle bottom inner areas are in tension. The maximum tensile stresses are at the 700 MPa level for these three ceramic nozzles. If any of these ceramics have tensile strengths smaller than 700 MPa, cracks or material separations can be expected to occur.

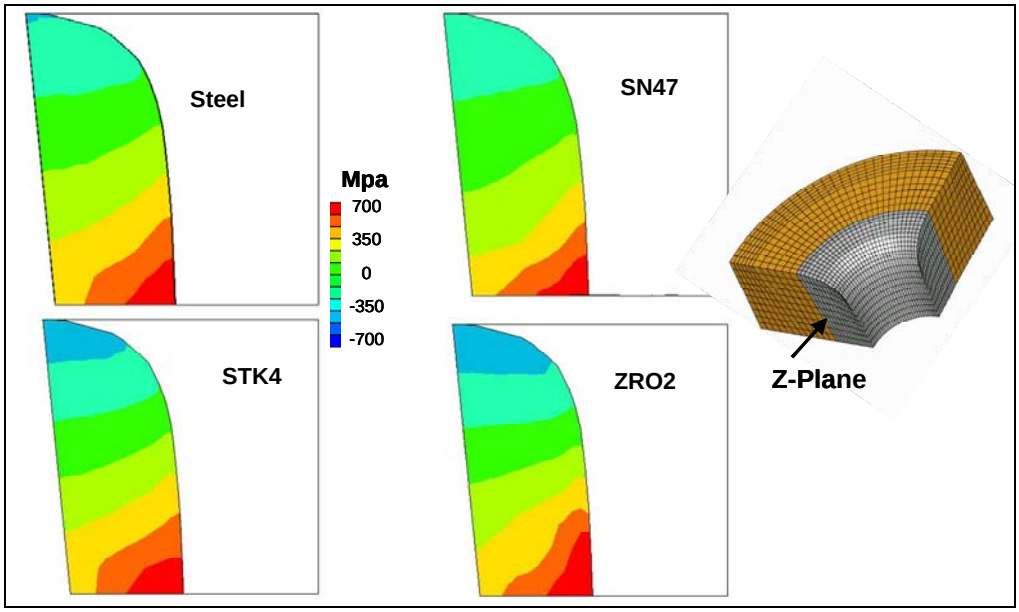

Figure 11. The hoop stress contours for the steel and ceramic nozzles plotted in the z-plane (see the appendix).

Once the maximum tensile stress locations are determined, the stress profiles at these points can be plotted in time; these are given in figure 12. The hoop stresses are subjected to tensile stress over the entire dynamic response time for the steel and ceramic nozzles. The radial stresses, by contrast, are always in compression and peak near 350 MPa.

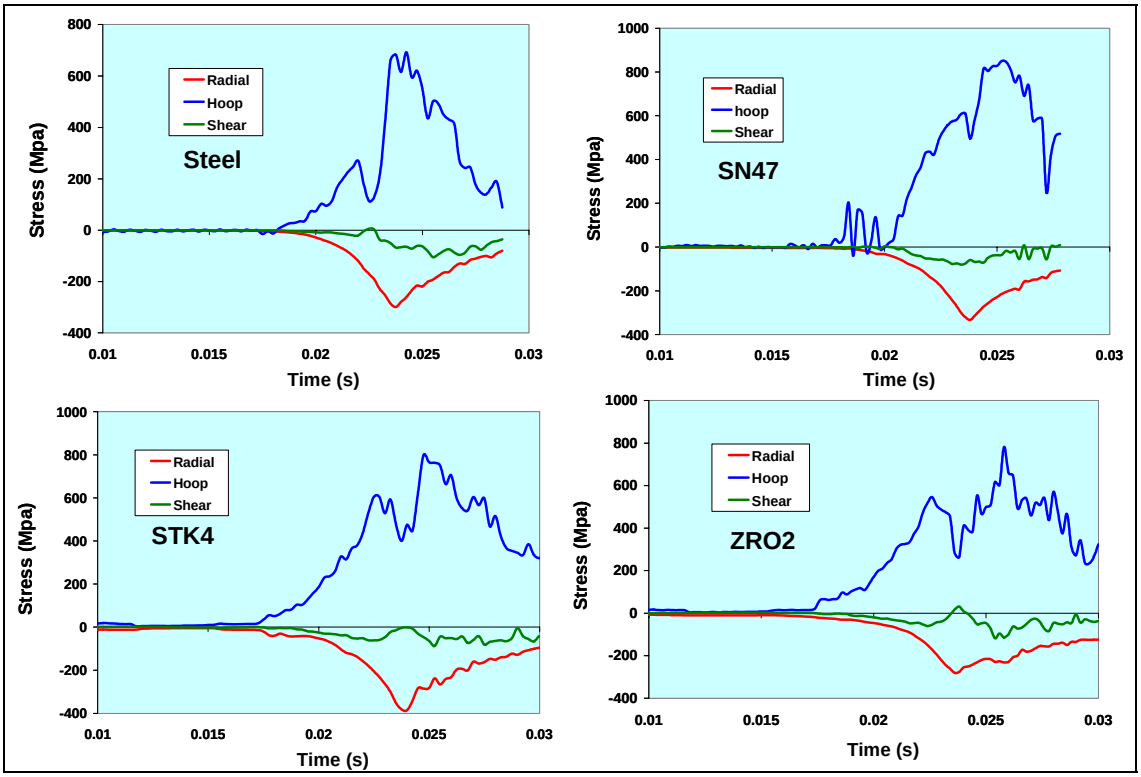

Figure 12. The steel and ceramic nozzle dynamic stress profiles.

From the previous discussion, the nozzle hoop stresses seem to play crucial roles in material selections and nozzle designs. Further comparisons and discussion will be given in the next section.

7. The Comparisons of Thermal and Dynamic Stress

For the comparisons, the contours from the thermal hoop stress and dynamic hoop stresses at their peak values are plotted in figure 13 for the steel nozzle. Obviously, they have different stress distributions. For the thermal hoop stress, the stress gradient is along the surface normal towards the inside of the nozzle. The maximum stress occurs in the nozzle entrance area. The gradient is sharp at 15 GPa per mm in compression. For the dynamic stress, the stress gradient is in compression at the top of the nozzle and in tension at the bottom. The maximum tension stress occurs at the nozzle inner corner at a value near 700 MPa, which may cause ceramic nozzle fracture failures.

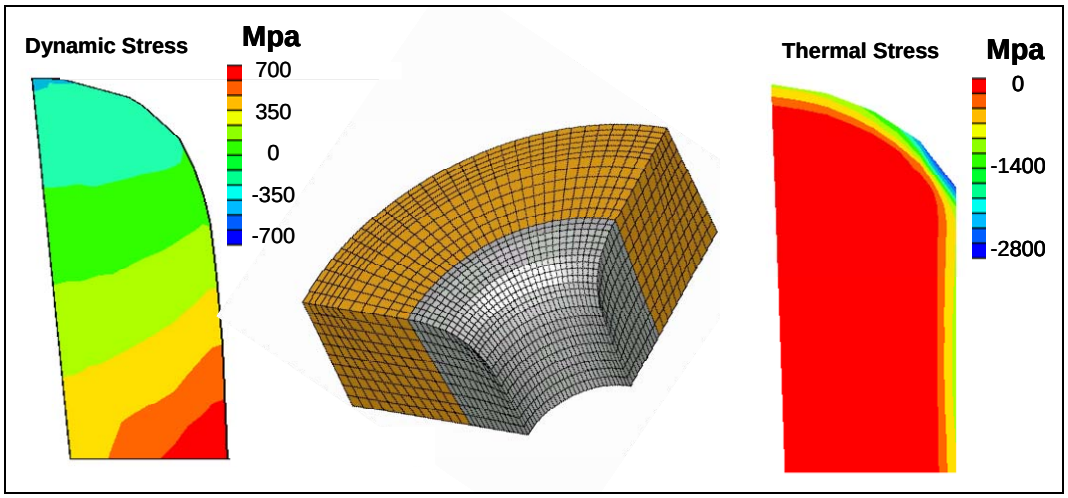

Figure 13. The hoop stress features for the thermal and dynamic loads.

Since the nozzle is subjected to both thermal and dynamic loads in the test, their peak values may not occur at the same time and the stress signs may be opposite for the transient stress cases. The combined effect has to be considered. Since both thermal and dynamic analyses are based on linear assumptions, the total result is the superposition of both corresponding individual results. Figure 14 shows the thermal and dynamic hoop stress profiles in the steel nozzle inner bottom corner area (maximum tensile stress location).

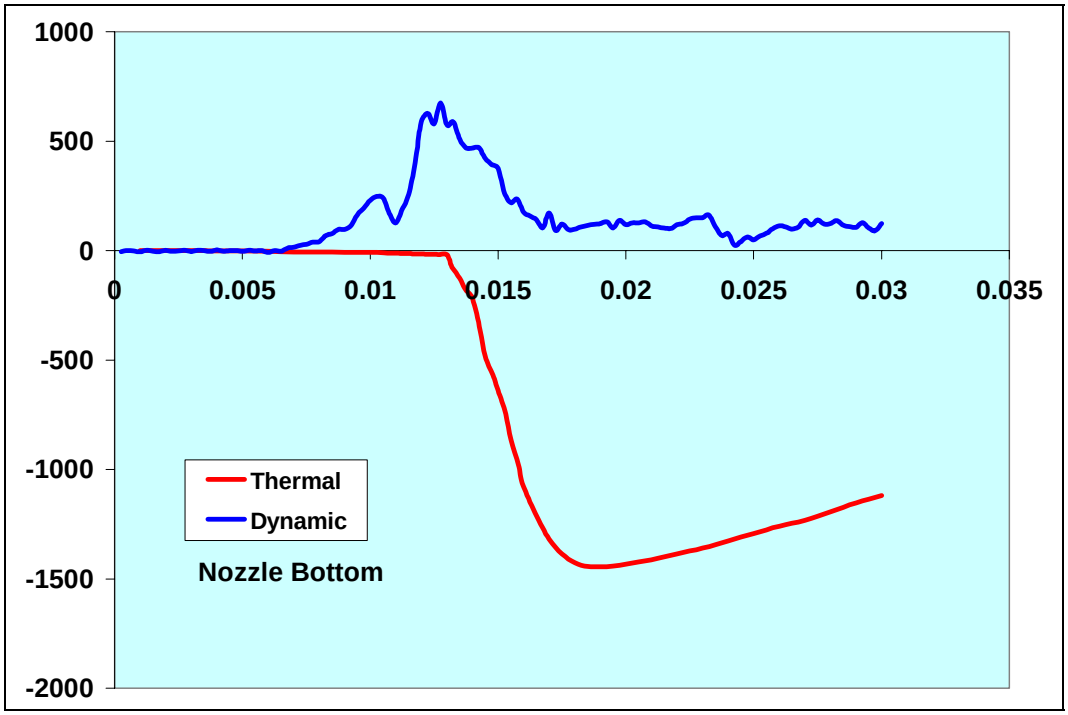

Figure 14. The transient thermal and dynamic hoop stresses.

From figure 14, it is seen that the peak thermal stress is delayed about 0.35 ms from the peak dynamic stress. Since their signs are opposite, the dynamic tension stress partially offsets the thermal compressive stress. Since the peak tension stress occurs at 1.25 ms, the maximum tensile stress is not markedly reduced. Similar stress situations are found for the ceramic nozzles. In table 2, the peak values of stresses for steel and ceramic nozzles are summarized for both thermal and dynamic analyses.

Table 2. The summary table of peak thermal and dynamic stresses for the steel and ceramic nozzles.

Nozzle Materials	**Radial (MPa)**	**Hoop (MPa)**	**Shear (MPa)**
Steel (thermal)	520 (compressive)	2890 (compressive)	895
Steel (dynamic)	310 (compressive)	1770 (tension)	100
SN47 (thermal)	325 (compressive)	1770 (compressive)	55
SN47 (dynamic)	345 (compressive)	825 (tension)	70
STK4 (thermal)	270 (compressive)	1430 (compressive)	460
STK4 (dynamic)	375 (compressive)	825 (tension)	80
ZR02 (thermal)	825 (compressive)	4050 (compressive)	1340
ZR02 (dynamic)	310 (compressive)	750 (tension)	80

It is noted from the table that the hoop stresses for each material are dominant. They not only have the highest compressive stresses but also have the most noticeable tensile stress. For the three ceramic nozzles, they have the same level of dynamic tensile stress (750 and 825 MPa). However, the ZRO2 ceramic material has significantly higher compressive thermal hoop stress at a value of 4050 MPa. Relatively, the SN47 and STK4 ceramics have lower thermal compressive stresses at vales of 1770 and 1430 MPa, respectively.

8. Conclusion

Three ceramic nozzles, SN47, STK4, and ZRO2, have been investigated and compared with a traditional steel nozzle. The ABAQUS FEM code is used for thermal stress analysis and the DYNA3D FEM code is used for dynamic stress analysis. In the thermal stress analysis, the temperature histories previously obtained for each material are sequentially input into transient stress analysis. The thermal stress distributions and profiles for the steel and ceramic nozzles are obtained. The fully-coupled thermal stress analysis was performed and shown to produce nearly identical results for the sequentially-coupled analysis. In the dynamic analysis, the interior ballistic pressure is applied to the nozzles. The dynamic responses show significant tensile hoop stresses for all the steel and ceramic nozzles. The thermal stresses are all limited in compression for the nozzles. Both maximum thermal hoop stresses and dynamic tensile stresses of steel and ceramic nozzles are given in table 2. ZRO2 ceramics have the highest thermal compressive hoop stress. These stress results are essential for design, test, and reference purposes.

9. References

1. Swab, J. J.; Wereszczak, A. A. *Mechanical and Thermal Properties of Advanced Ceramics for Gun Barrel Applications*; ARL-TR-3417; U.S. Army Research Laboratory: Aberdeen Proving Ground, MD, 2005.

2. Underwood, J. H.; Todaro, M. E.; Vigilante, G. N. *Modeling of Transient Thermal Damage in Ceramics for Cannon Bore Applications*; U.S. Army Armament Research, Development and Engineering Center, Benet Laboratories: Watervliet, NY, 2004.

3. *ABAQUS/Standard User's Manual*; version 6.4; Hibbitt, Karlsson and Sorensen, Inc.: Pawtucket, RI, 2003.

4. Whirley, R. G.; Engelmann, B. E. *DYNA3D –A Nonlinear, Explicit, Three-Dimensional Finite Element Code for Solid and Structure Mechanics*; UCRL-MA-107254 Rev. 1; Lawrence Livermore National Laboratory: Livermore, CA, November 1993.

5. Huang, X.; Garner, J.; Conroy, P. *Thermal Analysis for a 37-mm Gun Chamber with Ceramic Nozzles*; ARL-MR-624; U.S. Army Research Laboratory: Aberdeen Proving Ground, MD, 2005.

6. Baumeister, T.; Avallone, E. *Standard Handbook for Mechanical Engineers*; 8th ed.; Kingsport Press, Inc.: New York City, NY, 1979.

7. Timoshenko, G. *Theory of Elasticity*; 3rd ed.; McGraw-Hill Companies: New York, NY, 1970; p 224.

8. Conroy, P. *Vented Fixture Modeling*; ARL-TR-2952; U.S. Army Research Laboratory: Aberdeen Proving Ground, MD, 2003.

INTENTIONALLY LEFT BLANK.

Appendix. The Stress Relationship Between the Polar and Cartesian Coordinate Systems

The general relationship between Polar and Cartesian coordinate systems for the stress components is shown in the following transformation matrix. For special cases, when the angle θ equals to 0° or 90°, the relations in figure A-1 pertain.

$$\begin{bmatrix} \sigma_r \\ \sigma_\theta \\ \tau_{r\theta} \end{bmatrix} = \begin{bmatrix} c^2 & s^2 & 2sc \\ s^2 & c^2 & -2sc \\ -sc & sc & c^2-s^2 \end{bmatrix} \begin{bmatrix} \sigma_z \\ \sigma_y \\ \tau_{zy} \end{bmatrix}, \qquad \text{(A-1)}$$

where C = cosθ and S = sinθ.

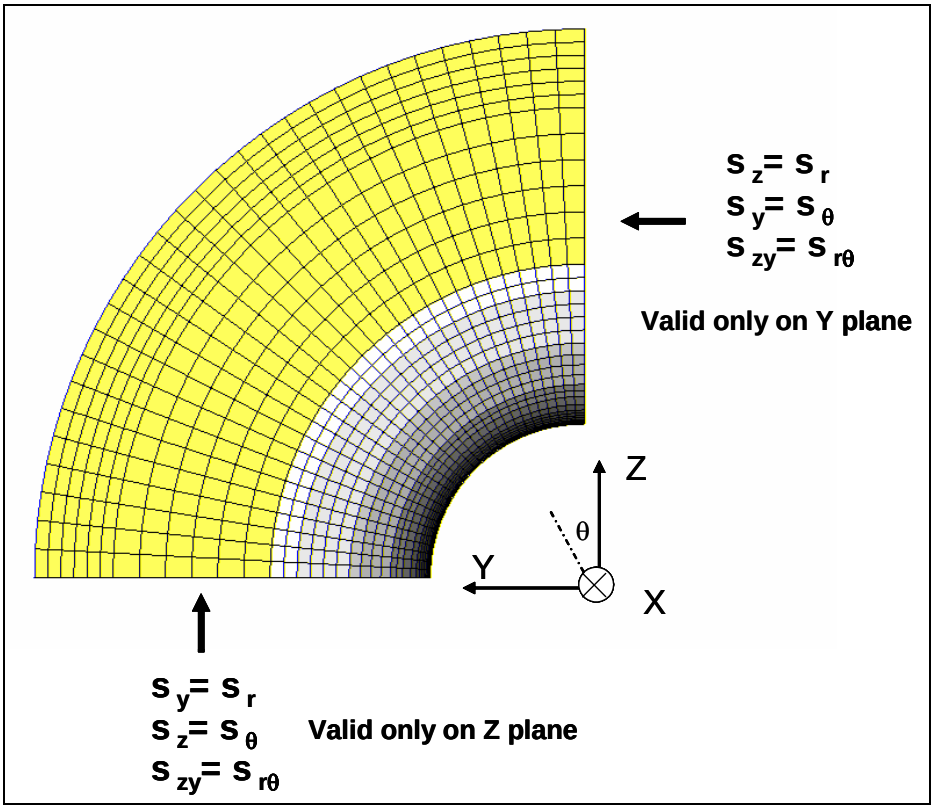

Figure A-1. Stress relationship between Polar and Cartesian coordinate systems.

NO. OF
COPIES ORGANIZATION

1 (PDF ONLY) DEFENSE TECHNICAL INFORMATION CTR
DTIC OCA
8725 JOHN J KINGMAN RD
STE 0944
FORT BELVOIR VA 22060-6218

1 US ARMY RSRCH DEV & ENGRG CMD
SYSTEMS OF SYSTEMS INTEGRATION
AMSRD SS T
6000 6TH ST STE 100
FORT BELVOIR VA 22060-5608

1 INST FOR ADVNCD TCHNLGY
THE UNIV OF TEXAS
AT AUSTIN
3925 W BRAKER LN
AUSTIN TX 78759-5316

1 DIRECTOR
US ARMY RESEARCH LAB
IMNE ALC IMS
2800 POWDER MILL RD
ADELPHI MD 20783-1197

3 DIRECTOR
US ARMY RESEARCH LAB
AMSRD ARL CI OK TL
2800 POWDER MILL RD
ADELPHI MD 20783-1197

ABERDEEN PROVING GROUND

1 DIR USARL
AMSRD ARL CI OK TP (BLDG 4600)

NO. OF COPIES ORGANIZATION

1 HQDA
DAMO FDT
400 ARMY PENTAGON
WASHINGTON DC 20310-6218

1 DARPA
SPECIAL PROJECTS OFFICE
J CARLINI
3701 N FAIRFAX DR
ARLINGTON VA 22203-1714

1 DIRECTOR
US ARMY RESEARCH LAB
AMSRD ARL D
J MILLER
2800 POWDER MILL RD
ADELPHI MD 20783-1197

1 HQDA DIR R&D
SAAL TR
W MORRISON
SUITE 9800
2511 JEFFERSON DAVIS HWY
ARLINGTON VA 22201

1 HQ US ARMY MATERIEL CMD
9301 CHAPEK RD
FORT BELVOIR VA 22060-5527

1 US ARMY BMDS CMD
ADVANCED TECHLGY CTR
PO BOX 1500
HUNTSVILLE AL 35807-3801

1 OFC OF THE PRODUCT MGR
SFAE AR HIP IP
R DE KLEINE
PICATINNY ARSENAL NJ 07806-5000

1 CDR US ARMY ARDEC
PROD BASE MODRNZTN AGENCY
AMSMC PBM
A SIKLOSI
PICATINNY ARSENAL NJ
07806-5000

1 CDR US ARMY ARDEC
PROD BASE MODRNZTN AGENCY
AMSTA AR WES
L LAIBSON
PICATINNY ARSENAL NJ
07806-5000

NO. OF COPIES ORGANIZATION

3 PM PEO ARMAMENTS
TANK MAIN ARMAMENT SYS
AMCPM TMA
AMCPM TMA 105
AMCPM TMA AS
H YUEN
PICATINNY ARSENAL NJ
07806-5000

2 CDR US ARMY ARDEC
AMSTA AR CCH B
C MANDALA
E FENNELL
PICATINNY ARSENAL NJ
07806-5000

1 CDR US ARMY ARDEC
AMSTA AR CCS
PICATINNY ARSENAL NJ
07806-5000

1 CDR US ARMY ARDEC
AMSTA AR WE
PICATINNY ARSENAL NJ
07806-5000

2 PM MAS
SFAE AMO MAS SMC
PICATINNY ARSENAL NJ
07806-5000

1 COMMANDER
US ARMY ARDEC
AMSTA AR CCH P
J LUTZ
PICATINNY ARSENAL NJ
07806-5000

3 CDR US ARMY ARDEC
ST A AR AEE WW
M MEZGER
D WIEGAND
P LU
PICATINNY ARSENAL NJ
07806-5000

1 CDR US ARMY ARDEC
AMSTA AR DB ST
G FERDINAND
PICATINNY ARSENAL NJ
07806-5000

NO. OF COPIES	ORGANIZATION
9	CDR US ARMY ARDEC AMSTA AR WEE S EINSTEIN S WESTLEY S BERNSTEIN J RUTKOWSKI B BRODMAN P OREILLY R CIRINOONE P HUI J OREILLY PICATINNY ARSENAL NJ 07806-5000
1	CDR US ARMY ARDEC AMSTA AR FS T GORA PICATINNY ARSENAL NJ 07806-5000
1	CDR US ARMY ARDEC AMSTA AR FS DH PICATINNY ARSENAL NJ 07806-5000
2	CDR US ARMY ARDEC AMSTA AR FS AS R KOPMANN B MACHAK PICATINNY ARSENAL NJ 07806-5000
1	CDR US ARMY ARDEC AMST A AR FSA D K CHUNG PICATINNY ARSENAL NJ 07806-5000
1	DIR BENET WEAPONS LAB AMSTA AR CCB T S SOPOK WATERVLIET NY 12189-4050
1	DIR BENET WEAPONS LAB AMSTA AR CCB TA M AUDINO WATERVLIET NY 12189-4050
1	DIR BENET WEAPONS LAB AMSTA AR CCB D R HASENBEIN WATERVLIET NY 12189-4050

NO. OF COPIES	ORGANIZATION
2	CDR US ARMY RSRCH OFC TECH LIB D MANN PO BOX 12211 RESEARCH TRIANGLE PARK NC 27709-2211
1	PM US ARMY TANK AUTOMOTIVE CMD AMCPM ABMS T DEAN WARREN MI 48092-2498
1	PM US ARMY TANK AUTOMOTIVE CMD FIGHTING VEHICLES SYSTEMS SFAE ASM BV WARREN MI 48397-5000
1	PM US ARMY TANK AUTOMOTIVE CMD ABRAMS TANK SYSTEM SFAE ASM AB WARREN MI 48397-5000
1	DIR HQ TRAC RPD ATCD MA FT MONROE VA 23651-5143
1	CDR RADFORD ARMY AMMUNITION PLANT SMCAR QA HI LIB RADFORD VA 24141-0298
1	COMMANDANT USAFC&S ATSF CN P GROSS FT SILL OK 73503-5600
4	CDR NAVAL RSRCH LAB TECH LIBRARY CODE 4410 K KAILASANATE J BORIS E ORAN WASHINGTON DC 20375-5000

NO. OF COPIES	ORGANIZATION
1	OFFICE OF NAVAL RSRCH CODE 473 J GOLDWASSER 800 N QUINCY ST ARLINGTON VA 22217-9999
5	CDR NAVAL SURFACE WARFARE CTR S MITCHELL C MICHIENZI J CONSAGA C GOTZMER TECHLIB INDIAN HEAD MD 20640-5000
1	CDR NAVAL SURFACE WARFARE CTR CODE G30 GUNS & MUNITIONS DIV DAHLGREN VA 22448-5000
1	CDR NAVAL SURFACE WARFARE CTR CODE G32 GUNS SYSTEMS DIV DAHLGREN VA 22448-5000
1	CDR NAVAL SURFACE WARFARE CTR CODE E23 TECHLIB DAHLGREN VA 22448-5000
1	CDR NAVAL SURFACE WARFARE CTR R HUBBARD G33 DAHLGREN VA 22448-5000
2	CDR NAVAL AIR WARFARE CTR CODE 3895 T PARR R DERR CH1NA LAKE CA 93555-6001
1	CDR NAVAL AIR WARFARE CTR INFORMATION SCIENCE DIV CHINA LAKE CA 93555-6001

NO. OF COPIES	ORGANIZATION
1	WL MNME ENERGETIC MATERIALS BR 2306 PERIMETER RD STE9 EGLIN AFB FL 32542-5910
1	DIR SANDIA NATL LABS M BAER DEPT 1512 PO BOX 5800 ALBUQUERQUE NM 87185
1	DIR SANDIA NATL LABS COMBUSTION RSRCH FACILITY R CARUNG LIVERMORE CA 94551-0469
2	DIR LLNL L355 A BUCHINGHAM M FINGER PO BOX 808 LIVERMORE CA 94550-0622
1	CIA J BACKOFEN RM 4PO7 NHB WASHINGTON DC 20505
2	MILLERSVILLE UNIV PHYSICS DEPT C W PRICE M NOLAN MILLERSVILLE PA 17551
2	UNIV OF ILLINOIS DEPT OF MECH INDUSTRY ENGINEERING H KRIER R BEDDINI 144 MEB 1206 N GREEN ST URBANA IL 61801-2978
5	PENNSYLVANIA STATE UNIV DEPT OF MECHANICAL ENGRG V YANG K KUO S THYNELL G SETTLES R YETTER UNIVERSITY PARK PA 16802-7501
1	ARROW TECHLGY ASSOC INC 1233 SHELBURNE RD D 8 SOUTH BURLINGTON VT 05403

NO. OF COPIES ORGANIZATION

1 AAI CORPORATION
D CLEVELAND
PO BOX 126
HUNT VALLEY MD 21030-0126

2 ALLIANT TECHSYSTEMS INC
ALLEGHENY BALLISTICS LAB
W B WALKUP
T F FARABAUGH
PO BOX 210
ROCKET CENTER WV 26726

3 ALLIANT TECHSYSTEMS INC
C AAKHUS MN07 LW54
R DOHRN MN07 LW54
D KAMDAR MNO7 LW54
5050 LINCOLN DR
EDINA MN 55436

4 ALLIANT TECHSYSTEMS INC
RADFORD ARMY AMMO PLANT
D A WORRELL
W J WORRELL
S RITCHIE
K BROWN
RADFORD VA 24141-0299

3 ST MARKS POWDER
GENERAL DYNAMICS ARM SYS
J DRUMMOND
J HOWARD
R PULVER
7121 COASTAL HWY
CRAWFORDVILLE FL 32327

1 GENERAL DYNAMICS ARM SYS
J TALLEY RM 1305
LAKESIDE AVE
BURLINGTON VT 05401

1 PRIMEX
BADGER ARMY AMMO PLANT
F E WOLF
BARABOO WI 53913

4 PRIMEX
E J KIRSCHKE
A F GONZALEZ
J DRUMMOND
D W WORTHINGTON
PO BOX 222
SAINT MARKS FL 32355-0222

NO. OF COPIES ORGANIZATION

2 PRIMEX
N HYLTON
J BUZZETT
10101 9TH ST NORTH
ST PETERSBURG FL 33716

1 PAUL GOUGH ASSOC INC
P S GOUGH
1048 SOUTH ST
PORTSMOUTH NH 03801-5423

2 VERITAY TECHGY INC
R SALIZONI
J BARNES
4845 MILLERSPORT HWY
EAST AMHERST NY 14501-0305

1 PRIMEX
DIR LARGE CAL R&D
E STEINER
PO BOX 127
RED LION PA 17356

1 SRI INTERNATIONAL
TECH LIB
PROPULSION SCIENCES DIV
333 RAVENWOOD AVE
MENLO PARK CA 94025-3493

1 COMMANDING GENERAL
US ARMY MATERIEL CMD
AMCRDA TF
5001 EISENHOWER AVE
ALEXANDRIA VA 22333-0001

ABERDEEN PROVING GROUND

1 CDR USAATC
CSTE DTC AT SL
R HENDRICKSEN
APG MD 21005

31 DIR USARL
AMSRD ARL WM
B RINGERS
AMSRD ARL WM BC
P PLOSTINS
M BUNDY
J GARNER
P WEINACHT

NO. OF
COPIES ORGANIZATION

ABERDEEN PROVING GROUND

AMSRD ARL WM BD
W R ANDERSON
R A BEYER
A L BRANT
S W BUNTE
C F CHABALOWSKI
T P COFFEE
J COLBURN
P J CONROY
B E FORCH
B E HOMAN
S L HOWARD
P J KASTE
A J KOTLAR
C LEVERITT
K L MCNESBY
M MCQUAID
M S MILLER
A W MIZIOLEK
J B MORRIS
J A NEWBERRY
M J NUSCA
R A PESCE-RODRIGUEZ
G P REEVES
B M RICE
R C SAUSA
A W WILLIAMS

INTENTIONALLY LEFT BLANK.